

# Characterization of a $6\times 6\text{-mm}^2$ $75\text{-}\mu\text{m}$ cell MPPC suitable for the Cherenkov Telescope Array Project

G. Romeo<sup>a</sup>, G. Bonanno<sup>a</sup>, S. Garozzo<sup>a</sup>, A. Grillo<sup>a</sup>, D. Marano<sup>a</sup>, M. Munari<sup>a</sup>, M. C. Timpanaro<sup>a</sup>  
O. Catalano<sup>b</sup>, S. Giarrusso<sup>b</sup>, D. Impiombato<sup>b</sup>, G. La Rosa<sup>b</sup>, G. Sottile<sup>b</sup>

<sup>a</sup>INAF, Osservatorio Astrofisico di Catania, Via S. Sofia 78, I-95123 Catania (Italy)

<sup>b</sup>INAF, Istituto di Astrofisica Spaziale e Fisica cosmica di Palermo, Via U. La Malfa 153, I-90146 Palermo (Italy)

## Abstract

This paper presents the latest characterization results of a novel Low Cross-Talk (LCT) large-area ( $6\times 6\text{-mm}^2$ ) Multi-Pixel Photon Counter (MPPC) detector manufactured by Hamamatsu, belonging to the recent LCT5 family and achieving a fill-factor enhancement and cross-talk reduction. In addition, the newly adopted resin coating is demonstrated to yield improved photon detection capabilities in the 290-350nm spectral range, making the new LCT MPPC particularly suitable for emerging applications like Cherenkov Telescopes. For a  $3\times 3\text{-mm}^2$  version of the new MPPC under test, a comparative analysis of the large pixel pitch ( $75\text{-}\mu\text{m}$ ) detector versus the smaller pixel pitch ( $50\text{-}\mu\text{m}$ ) detector is also undertaken. Furthermore, measurements of the  $6\times 6\text{-mm}^2$  MPPC response versus the angle of incidence are provided for the characterized device.

*Keywords:* Silicon Photomultipliers, Detector Characterization, Photon Detection Efficiency, Angle of Incidence.

## 1. Introduction

Silicon photomultipliers (SiPMs) are a relatively new class of solid-state photodetectors suitable for an increasing number of perspective applications in many scientific fields. Thanks to their outstanding characteristics in terms of photon counting capability, low operating voltage, fast dynamic response and insensitivity to magnetic fields, SiPM applications have been continuously growing over time, especially in the fields of high-energy astrophysics [1]-[14], nuclear medicine [15]-[17] and cosmic-ray muon detection [18]-[20].

The unique features presented by most commercially available detectors from the world's leading manufacturers are the result of modern semiconductor fabrication technologies. Considerable effort is presently being invested by the producers of SiPMs to further improve the global performance achieved by this class of devices [21]-[25]. In addition, the large popularity of SiPMs in the sensors community has led to a remarkable number of characterization studies and methodologies for evaluating the detector performance [26]-[37]. The rising demand for optimal speed and single photon time resolution on one side, and for suitable integrated front-ends on the other, has also triggered research efforts for reliable analytical investigations on the dynamic response of SiPMs, allowing a detailed analytical description of the sensor behavior [38]-[44].

This paper presents the characterization of a newly available large-area ( $6\times 6\text{-mm}^2$ ) Multi-Pixel Photon Counter (MPPC) detector from Hamamatsu Photonics, addressing the challenge of high sensitivity and low cross-talk, especially requested in the new generation of Cherenkov telescopes as the ones adopted in the ASTRI Mini-Array Project [4] within the Cherenkov Telescope Array (CTA) Observatory [5]-[6].

We also present a comparative analysis of the large pixel pitch ( $75\text{-}\mu\text{m}$ ) detector versus the smaller pixel pitch ( $50\text{-}\mu\text{m}$ ) device with the same active area ( $3\times 3\text{-mm}^2$ ), to compare the detector performance when increasing the pixel dimension for the same device size. Furthermore, to investigate the  $6\times 6\text{-mm}^2$  detector response with respect to the incident photons, measurement at several angles of incidence are provided as well.

1 The measurements presented here are carried out at the Catania astrophysical Observatory Laboratory for Detectors  
2 (COLD) within INAF – Osservatorio Astrofisico di Catania.

## 3 2. Large-Area Low Cross-Talk MPPC Device

4 In the last few years, the advances in LCT technology have produced new generation MPPCs with improved char-  
5 acteristics and performance. New materials and processes have been adopted, achieving higher sensitivity and geomet-  
6 rical fill-factors. The optical trench improvement of the LCT detectors compared to the prior MPPC series of the same  
7 family is a result of new types of trenches which enables cross-talk reduction. On the other hand, the fill-factor im-  
8 provement of the new MPPC series results from a functional optimization of the physical structure of the device (max-  
9 imization of the active area).

10 The characterized large-area MPPC described in this paper belongs to the latest device series manufactured by Ha-  
11 mamatsu Photonics, denominated Low Cross-Talk (LCT) family and reported as the MPPC S13360 series in the man-  
12 ufacturer datasheet<sup>1</sup>. It is a prototype device provided by the vendor to the COLD laboratory for testing and evaluation  
13 purposes. Table I reports the main features of the characterized detector.

14 **TABLE I**  
15 Main physical features of the characterized large-area MPPC detector

<b>device series</b>	S13360-6075CS
<b>cell pitch</b>	75 $\mu$ m
<b>device size</b>	6 $\times$ 6mm <sup>2</sup>
<b>microcells</b>	6400
<b>surface coating</b>	silicone resin
<b>fill-factor</b>	82%
<b>breakdown voltage*</b>	52.01V

16 \* at 25°C

17 Moreover, silicone resin coating has been used for this device to achieve higher quantum efficiency in the near ul-  
18 traviolet (NUV) spectral region. Since this kind of device is very fast and sensitive to the light in the 290-700nm  
19 wavelength range, it is particularly suitable for the detection of Cherenkov flashes.

## 20 3. Experimental Results

21 The electro-optical equipment used for SiPM measurements is described in [26]. The main element of the front-end  
22 electronics for SiPM characterization is the Cherenkov Imaging Telescope Integrated Read-Out Chip (CITIROC) [45]-  
23 [47], which is an advanced version of the Extended Analogue SiPM Integrated Read-Out Chip (EASIROC) [48]-[51],  
24 both produced by WEEROC<sup>2</sup>. The modifications to CITIROC stem from INAF and originated from the design of the  
25 ASTRI SST-2M telescope camera [2]-[3]. To provide a versatile interface between the SiPM terminals and the CITI-  
26 ROC evaluation board, specific mechanical and electrical adapters have been fabricated, allowing several functional  
27 tests and measurements for SiPM characterizations to be performed. Temperature control and stabilization is obtained  
28 through a dedicated thermoelectric cooling system based on a Peltier cell; the entire cooling system is thermally cali-  
29 brated and can achieve temperatures from 10°C to 30°C. The mechanical housing is able to host various types of de-  
30 tectors by simply using a dedicated electronic adapter board.

31 Based on the equipment mentioned above, experimental measurements on the large-area MPPC of the LCT series

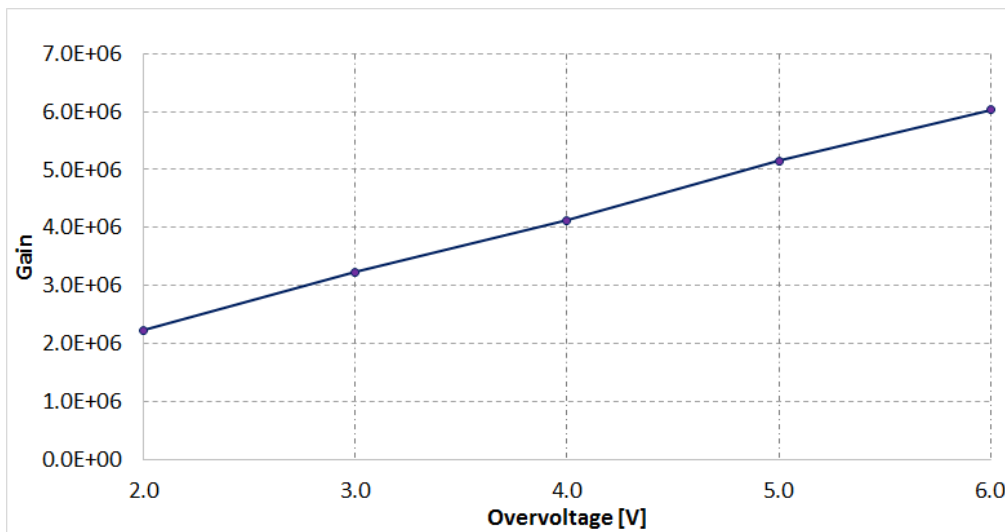
<sup>1</sup> <http://www.hamamatsu.com/jp/en/product/category/3100/4004/4113/S13360-6075CS/index.html>

<sup>2</sup> <http://www.weeroc.com>

1 are presented here in terms of the main detector performance parameters, i.e. gain, dark count rate, cross-talk and Pho-  
2 ton Detection Efficiency (*PDE*).

### 3 A. Gain

4 In order to evaluate the MPPC gain at a fixed temperature and in a specific range of operating voltages, charge am-  
5 plitude histograms are produced while illuminating the SiPM detector with a LED laser source of adjustable intensity  
6 and duration. By computing the average spacing between subsequent charge peaks in terms of Analog-to-Digital Con-  
7 verter (ADC) channels, and scaling for the constant ADC rate (charge/channel) and amplification factor, the SiPM  
8 gain is obtained for a fixed bias condition. A detailed description of the apparatus and the adopted technique can be  
9 found in [28]. The resulting measured gain data points, as a function of the applied overvoltage (*OV*) at 25°C are re-  
10 ported in Figure 1 for the characterized detector.



11  
12 Figure 1. Gain measurements of the characterized S13360-6075CS detector as a function of the applied overvoltage, at 25°C.

13 The expected linear trend of the gain as a function of the overvoltage is observed. Gain values higher than  $2 \times 10^6$   
14 are obtained in the analyzed overvoltage range.

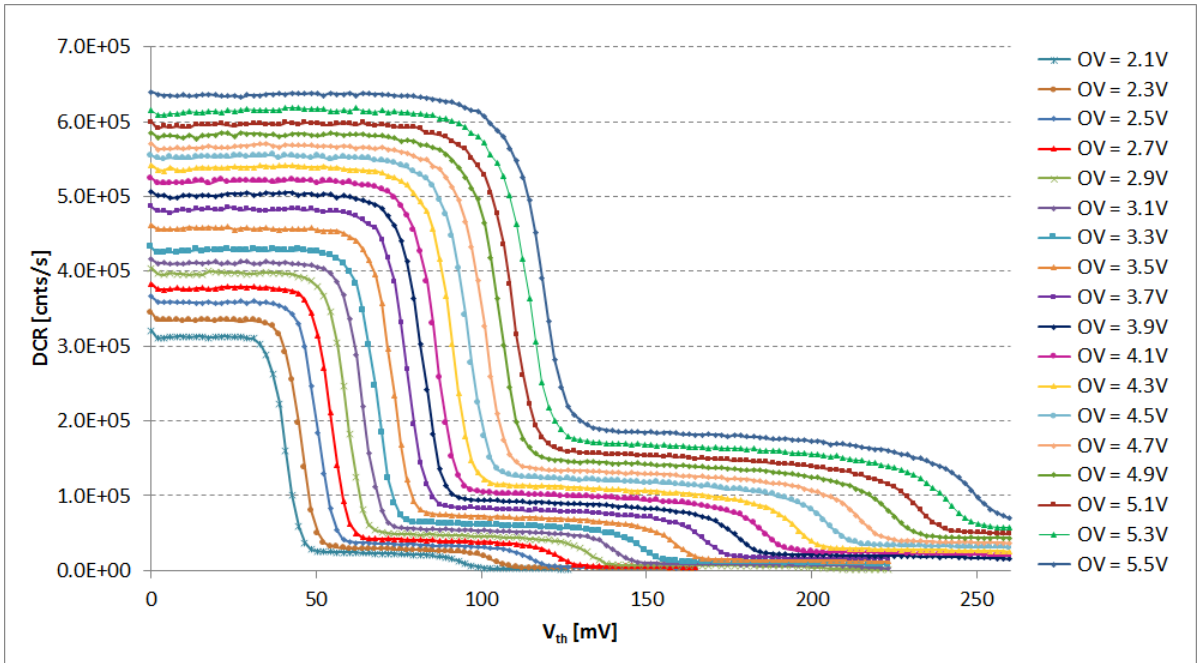
### 15 B. Dark Count Rate and Cross-Talk

16 The Dark Count Rate (*DCR*), at a selected threshold level, is essentially defined as the number of avalanche pulses  
17 produced by hot carriers, resulting in events that are perfectly equivalent to the signal from real photons.

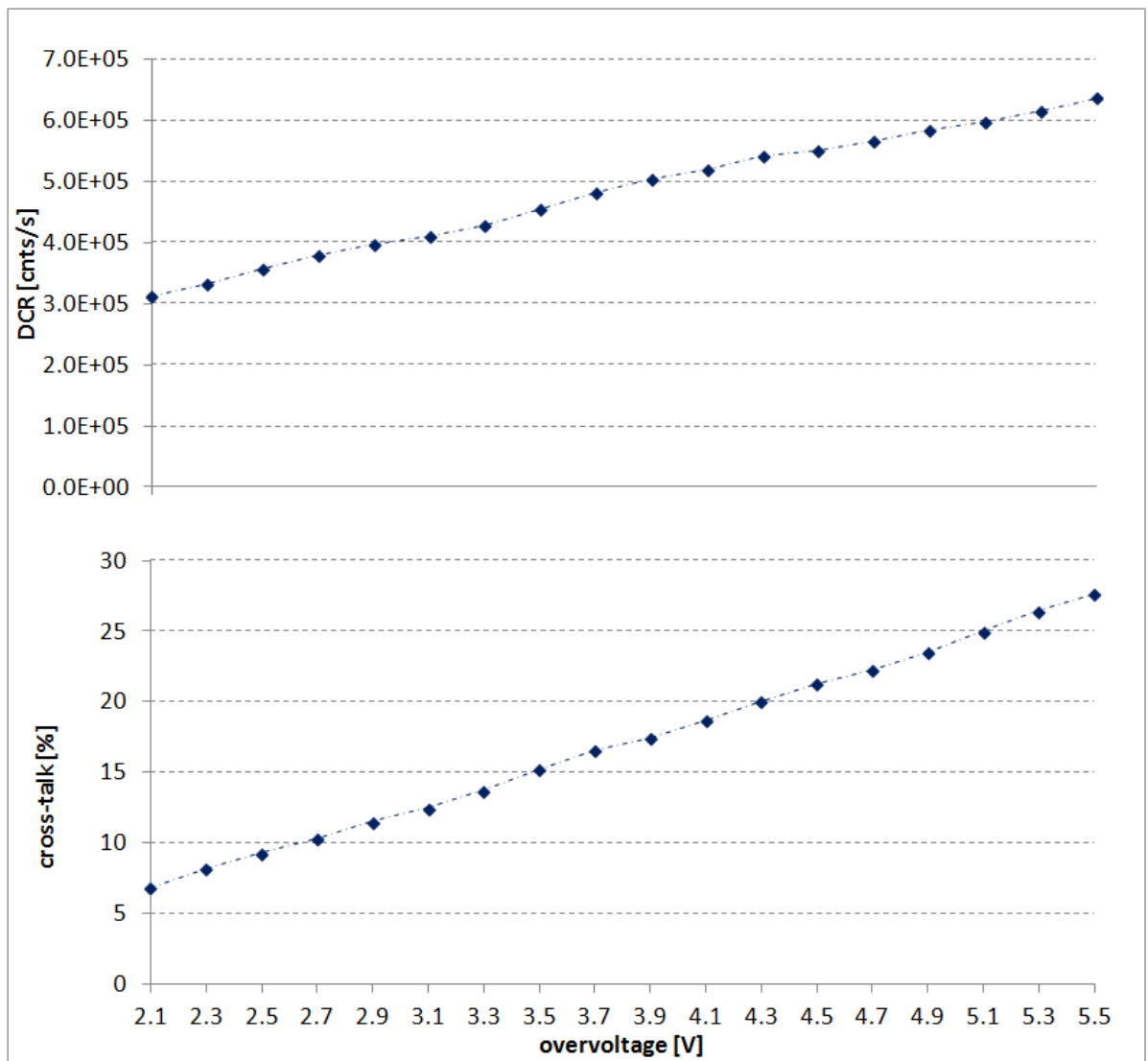
18 For a threshold above the electronics noise and below the photo-electron (*pe*) amplitude, all thermally generated  
19 avalanches are counted, as well as tunnel-assisted generated charge, afterpulsing and indirect optical cross-talk (extra-  
20 charge noise).

21 SiPM optical cross-talk, as reported in literature ([25], [27]), is evaluated as the ratio of the *DCR* at 1.5*pe* with re-  
22 spect to that at 0.5*pe*. This approach is based on the assumption that the probability of triggering two uncorrelated ava-  
23 lanches at the same time is negligible.

24 Figure 2 shows the *DCR* curves (also known as staircase functions) for the characterized LCT detector as a function  
25 of the discriminator threshold and for overvoltage values from 2.1V up to 5.5V, in steps of 200mV. Figure 3 reports  
26 the measured *DCR* and cross-talk probability as a function of the overvoltage.



1  
2 Figure 2. Staircase measurements of the characterized S13360-6075CS detector as a function of the discriminator threshold, at 25°C.



3  
4 Figure 3. DCR and cross-talk of the characterized S13360-6075CS detector as a function of the overvoltage, at 25°C.

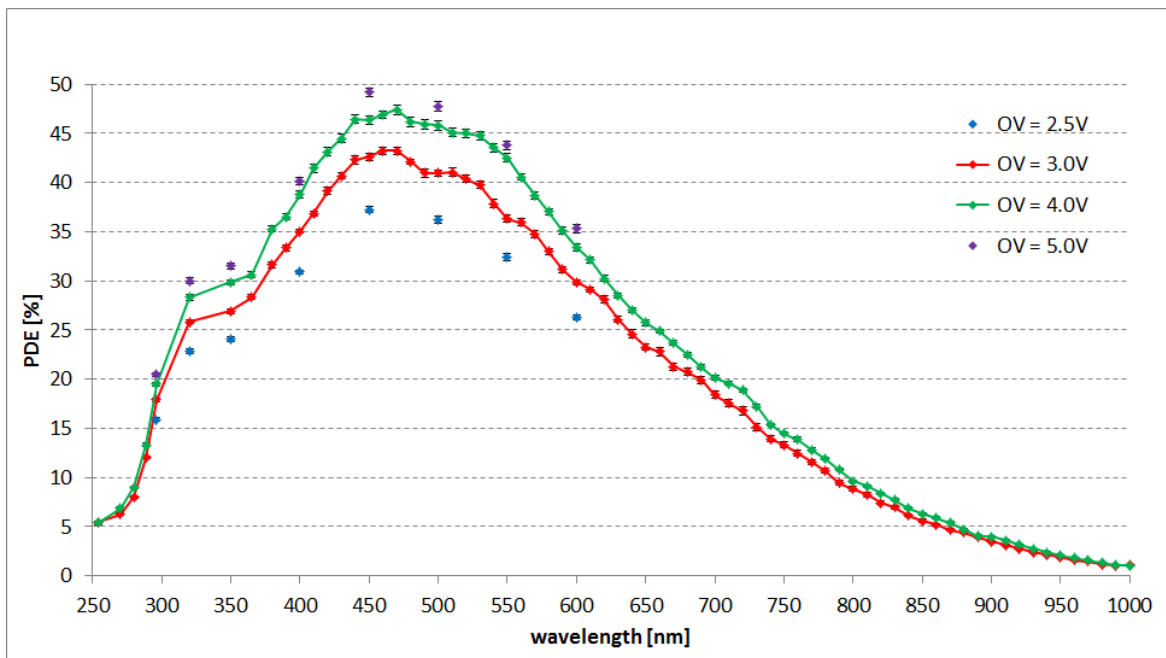
1 It can be observed that, in the analyzed overvoltage range, the *DCR* of the 6×6-mm<sup>2</sup> device remains lower than  
 2 700kHz. On the other hand, for a typical 3-V overvoltage operation, the cross-talk probability is around 12%, due to  
 3 the effects of the improved optical trenches adopted with respect to previous MPPC families [27].

### 4 C. Photon Detection Efficiency

5 SiPM absolute *PDE* measurements are carried out based on the photon counting method [27]-[29], by which the  
 6 number of pulses per unit time in monochromatic light conditions are compared to the light level recorded by a refer-  
 7 ence NIST photodetector at the same time, and this process is then repeated for several wavelengths.

8 It is worth noting that the adopted photon counting technique for determining the detector *PDE* is insensitive to the  
 9 optical cross-talk, as a 0.5-pe threshold is applied to all triggered pulses, so that simultaneous pulses are measured as a  
 10 single pulse. However, the obtained *PDE* results are not immune to extra-charge noise (indirect cross-talk and after-  
 11 pulsing), and therefore may be slightly overestimated.

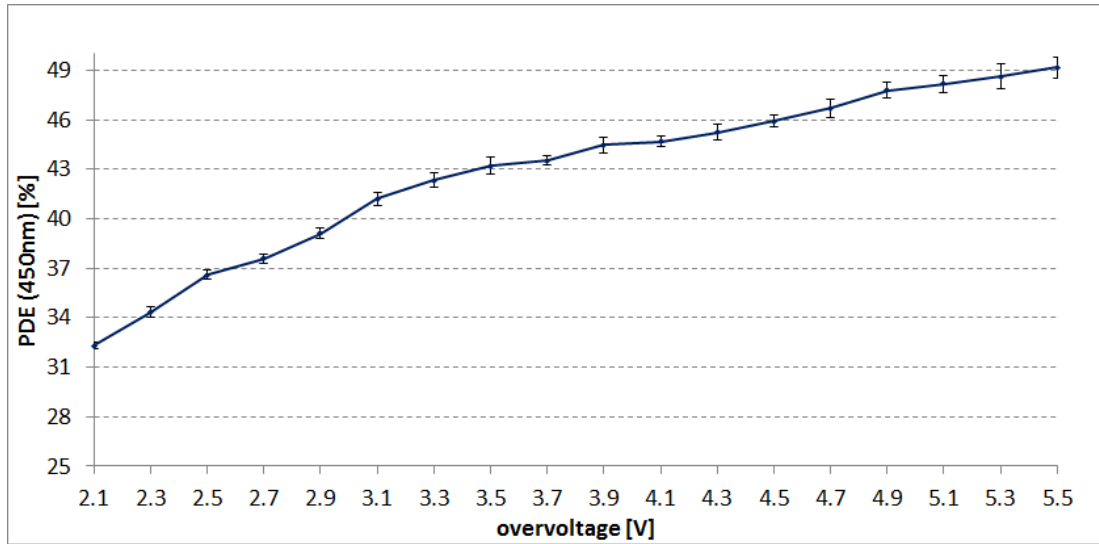
12 *PDE* measurements in the 250-1000-nm wavelength range are reported in Figure 4. The 290-350-nm range is par-  
 13 ticularly important in applications to detect Cherenkov light.



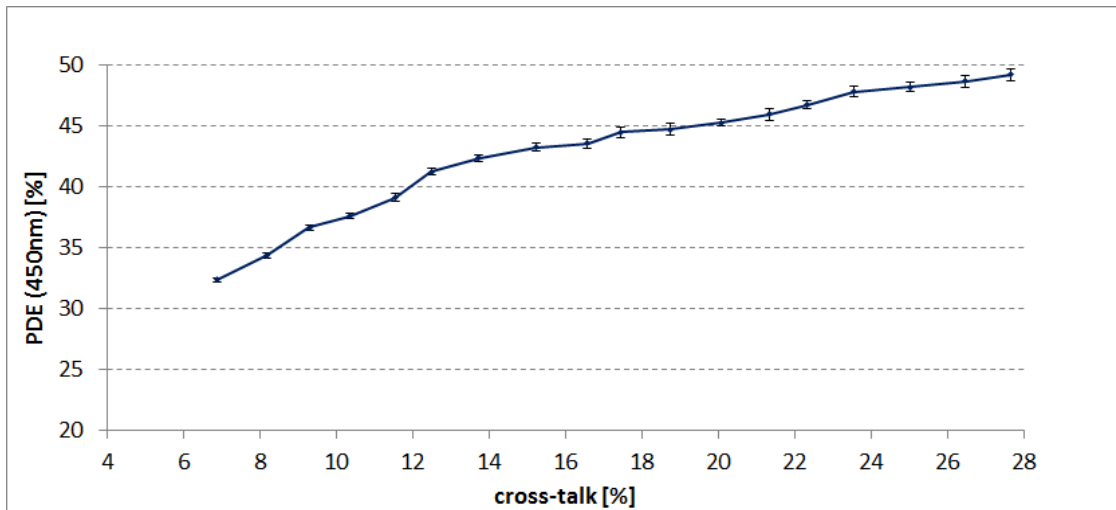
14  
 15 Figure 4. *PDE* measurements of the characterized S13360-6075CS detector at various overvoltages. Measurements at 3-V and 4-V overvoltage are  
 16 carried out in the 250-1000nm spectral range in steps of 10nm, while only eight points are shown for the other overvoltages.

17 The detector *PDE* at a 450-nm wavelength as a function of the applied overvoltage is shown in Figure 5. For rising  
 18 overvoltage values, a *PDE* of almost 50% can be obtained but, of course, at the expense of an increase in cross-talk;  
 19 furthermore, a progressive reduction in the *PDE* increase is observed at overvoltages higher than 3.5V.

20 In order to better quantify the detector performance, *PDE* measurements at 450nm as a function of cross-talk are  
 21 reported in Figure 6. Such a plot allows an evaluation of the optimal trade-off between *PDE* and cross-talk for the spe-  
 22 cific application. Data points in Figure 6 refer to the same overvoltage values as in Figure 5.



1  
2 Figure 5. *PDE* (450nm) versus the applied overvoltage for the S13360-6075CS detector.

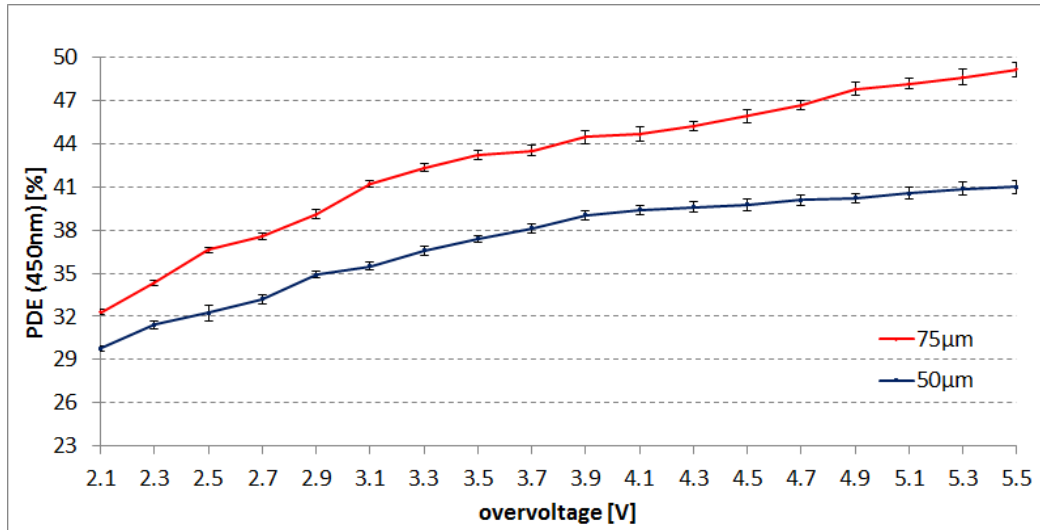


3  
4 Figure 6. *PDE* (450nm) versus the cross-talk for the S13360-6075CS detector.

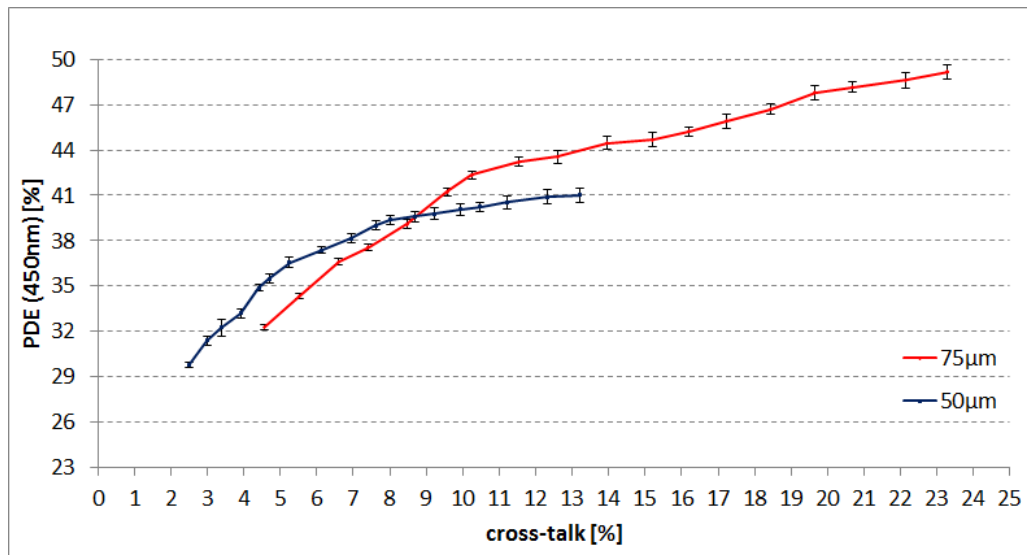
5 *D. 50- $\mu$ m vs. 75- $\mu$ m Pixel Pitch LCT MPPCs*

6 For a specific MPPC application, it is also important to evaluate the optimal trade-off between the detector *PDE*  
7 and cross-talk with respect to the pixel pitch. In fact, larger micro-pixels (better MPPC fill factor) means higher *PDE*  
8 but also implies a slightly increase in cross-talk probability. For these reasons, a comparative analysis of the large pix-  
9 el pitch (75- $\mu$ m) detector compared to the smaller (50- $\mu$ m) device for the same active area is believed to be particular-  
10 ly important.

11 As a large-area LCT MPPC with a 50- $\mu$ m pixel pitch is not presently available in our laboratory, the comparison is  
12 carried out using the 3 $\times$ 3-mm<sup>2</sup> detectors. Figure 7 depicts the *PDE* (450nm) curves as a function of the applied over-  
13 voltage for two 3 $\times$ 3-mm<sup>2</sup> MPPCs of the S13360 series and, in particular, the S13360-3075CS device, with a 75- $\mu$ m  
14 cell size, and the S13360-3050CS counterpart, with a 50- $\mu$ m active area. As can be noted, at overvoltages higher than  
15 3.5V, the 75- $\mu$ m pitch MPPC presents a *PDE* value that is between 8% and 9% higher than that of the 50- $\mu$ m pitch  
16 detector, which is compatible with the difference in fill factor of the two devices (82% for the 75- $\mu$ m detector against  
17 74% for the 50- $\mu$ m device). The difference in *PDE* between the two MPPCs gradually decreases at overvoltages lower  
18 than 3V. A better and more significant comparison is given by the *PDE* plots (at a wavelength of 450nm) in Figure 8  
19 as a function of the cross-talk.



1  
2 Figure 7. *PDE* (450nm) of the 50-µm and 75-µm LCT detectors as a function of the applied overvoltage.



3  
4 Figure 8. *PDE* (450nm) versus the cross-talk for the 50-µm and 75-µm LCT detectors.

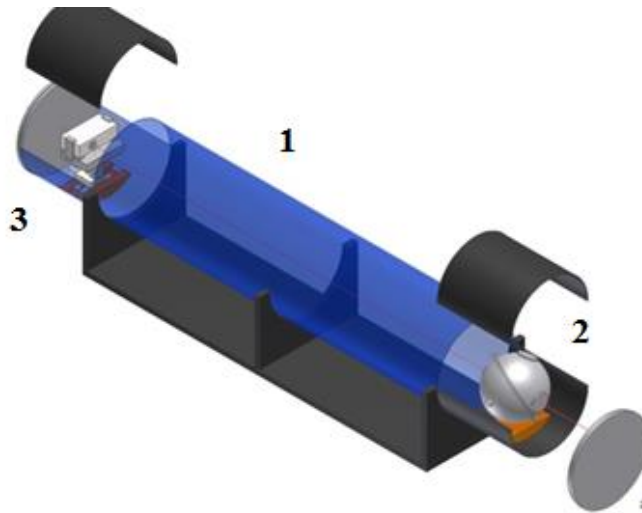
5 As can be observed comparing the two curves, while the S13360-3050CS MPPC is characterized by a lower cross-  
6 talk in the 30-40% *PDE* range, the S13360-3075CS device gives a higher *PDE* at greater cross-talk values. The two  
7 MPPCs present almost the same *PDE* value (39.5%) at a cross-talk of 8.5%. In applications where a cross-talk of  
8 ~20% is acceptable, a *PDE* of about 48% can be achieved only by the S13360-3075CS device. On the other hand, the  
9 50-µm pitch device is preferable where low cross-talk values are required.

10 **4. Response versus Angle of Incidence Measurements**

11 In this section, the 6×6-mm<sup>2</sup> MPPC response versus the incidence radiation angle is addressed.

12 *A. Measurement Set-Up*

13 Measurements of the MPPC Photon Response (*PR*) versus the Angle of Incidence (*AoI*) have been performed using  
14 the experimental set-up illustrated in Figure 9.



1



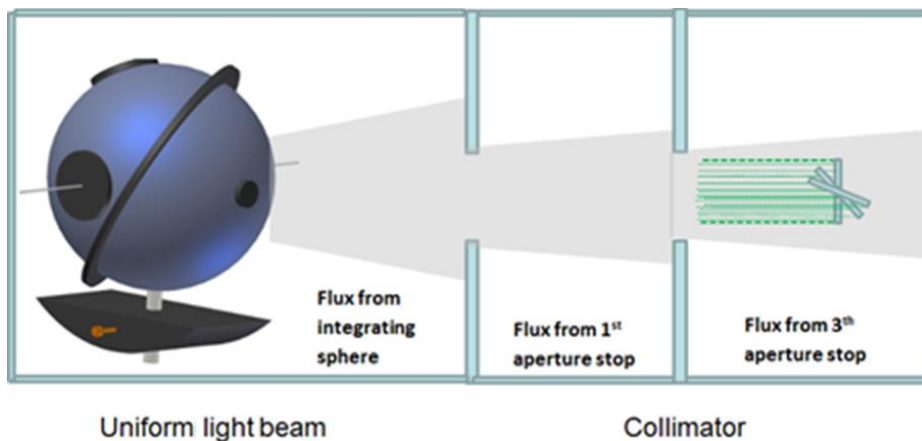
2

3 Figure 9. Experimental set-up for the angle of incidence measurements. In the upper panel, a 3D view of the system: 1. the tube; 2. source and integrating sphere; 3. the PSAU-CAEN system. In the lower panel, photograph of the actual system.

5 It consists of a PSAU-SiPM assembly [28], a light source with a high degree of uniformity and a 2-m long PVC cylindrical light-tight enclosure. The source is a green LED (568-nm wavelength), feeding a Labsphere standard integrating sphere (mod. IS-080, 8-inch diameter), that gives a uniform irradiance at the output port.

8 To obtain a collimated beam we introduced two diaphragms of 5 cm diameter along the tube. Taking into account the presence of these diaphragms, the length of the tube and the MPPC dimensions ( $6 \times 6 \text{ mm}^2$ ), the beam divergence is lower than 1 degree (see Figure 10).

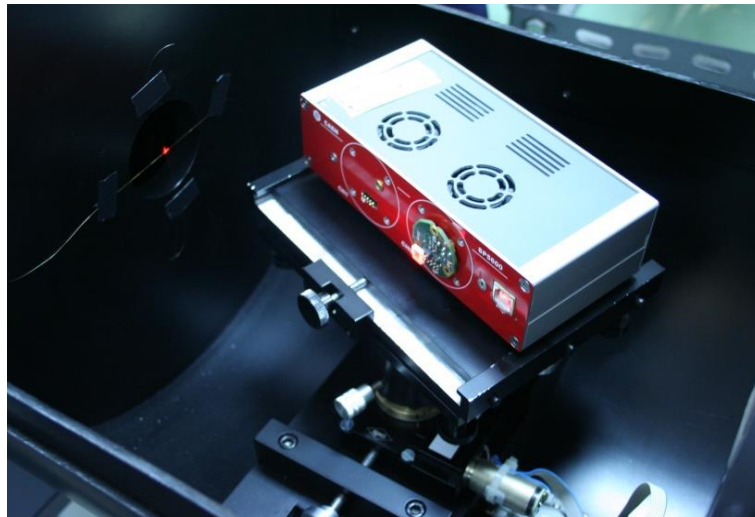
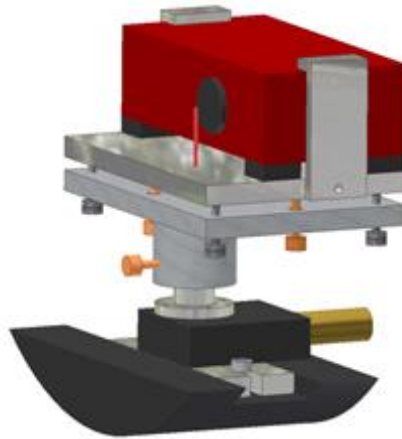
11



12

13 Figure 10. Schematic of the beam collimation system.

1 The PSAU-SiPM assembly is mounted on a mechanical system (see Figure 11) that allows the rotation of the SiPM  
2 around an axis parallel to the surface of the sensor and aligned with its center, obtaining a variation of the  $AoI$  of the  
3 beam with the detector. The rotary stage (OWIS DMT40-D20-HSM) can be controlled via computer, and permits a  
4 positional accuracy of 1/10 of a degree (from the manufacturer datasheet).



5  
6 Figure 11. Scheme of the PSAU-SiPM system mounted on stages (upper panel, 3D view of the rotary system; lower panel, photograph of the actual  
7 apparatus, showing the realized spot pointing at the detector surface).

8 The correct positioning of the SiPM with respect to the axis of rotation is assured by the presence of three linear  
9 stages that allow the translation of the SiPM itself: a laser beam is used to produce a spot on the surface of the detector  
10 and the linear stages are moved, checking that in rotating the system the spot does not move.

11 A fan mounted behind the PSAU-SiPM system ensures the removal/dispersal of the excess heat generated by the  
12 PSAU electronics.

### 13 *B. Measurement Results*

14 Once the system is mounted, the first operation is to define a raw zero position of the rotary stage. Due to the set-up  
15 geometry, the signal will have a cosine-like dependence on the  $AoI$ . Hence, the zero point of  $AoI$  (detector perpendic-  
16 ular to the beam) is defined as the rotary stage position for which a maximum signal is recorded.

17 The second step was to record the  $DCR$  at 0.5pe when the source was switched off. The  $DCR$  has been measured  
18 not only at the zero position, but also at different positions of the rotary stage: this has been done to take into account  
19 contributions to the signal due to light leakages in the enclosure. To guarantee stability of the LED emission, and thus  
20 avoid signal fluctuations, the source is turned-on one hour before measurements.

1 The raw signal  $RS(\theta)$  and dark signal  $DCR(\theta)$  have been recorded for each angular position  $\theta$  of the rotary stage,  
 2 with  $\theta$  ranging from -20 to +75 degrees, in steps of 5 degrees; The positive direction is arbitrary.

3 It should be noted that both  $RS(\theta)$  and  $DCR(\theta)$  are actually the mean values of 15 measurements and their  $\sigma_{RS}$  and  
 4  $\sigma_{DCR}$  correspond to the rms respect to the average.

5 From each pair of  $RS(\theta)$  and  $DCR(\theta)$  a net signal  $SN(\theta)$  has been calculated as:

$$6 \quad SN(\theta) = RS(\theta) - DCR(\theta) \quad (1)$$

8 The error on  $SN(\theta)$  has been estimated as:

$$9 \quad \sigma_{SN} = \sqrt{\sigma_{RS}^2 + \sigma_{DCR}^2} \quad (2)$$

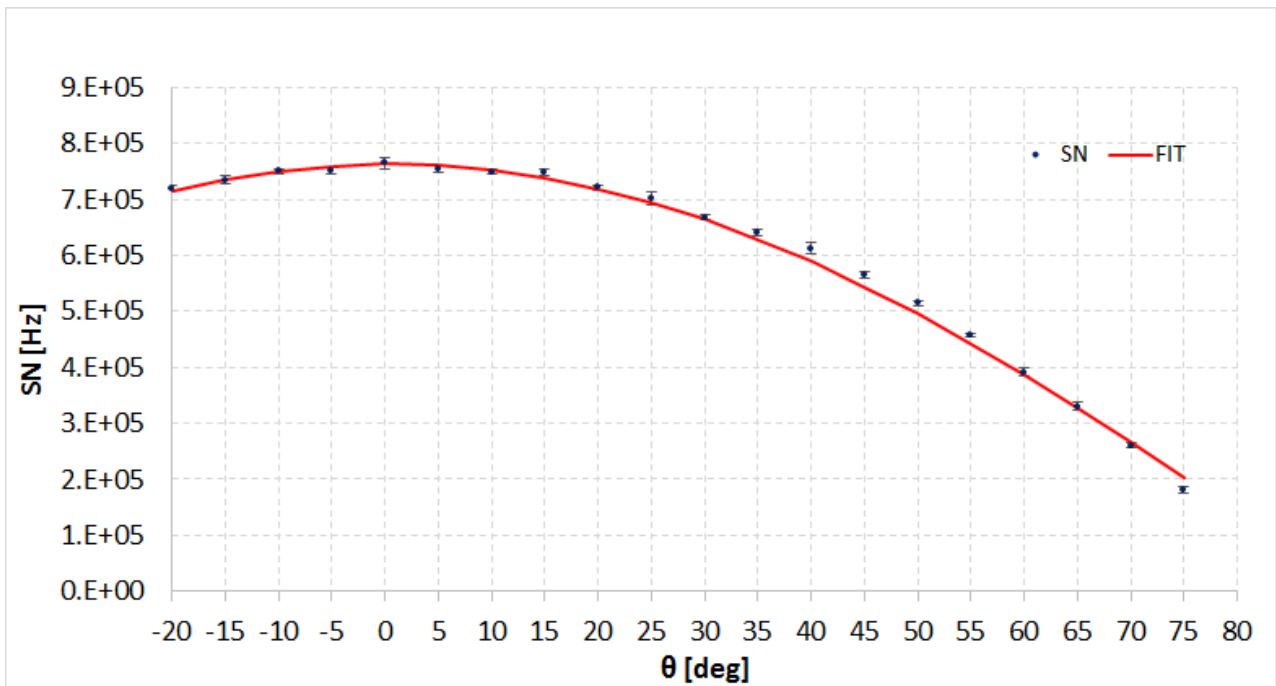
10 Since, as stated before, the measurements are expected to follow a cosine trend, they can be fit with a function of  
 11 the form:

$$12 \quad FIT(\theta) = SN_0 \cos(\theta + \theta_0) \quad (3)$$

13 where  $\theta_0$  is the offset error in identifying the zero position of the rotary stage and  $SN_0$  is the value at the zero angle of  
 14 the net signal. We are assuming here that the error affecting the positioning of the angular stage is small with respect  
 15 to  $\theta_0$ .

16  $SN_0$  and  $\theta_0$  have been estimated using a Python MPFIT routine from the *astrolibpy* library<sup>3</sup>, and the results of the fit  
 17 ( $FIT$ ) can be seen in the plot reported in Figure 12.

18



19

20 Figure 12. Detected signal SN at 568 nm vs incidence angles (dark-blue points). The best fit model is plotted with the red line. Parameters of the fit  
 21 are  $SN_0=7.653E5\pm 5E2$  counts/s, and  $\theta_0=-0.69\pm 0.06$  degrees. Error bars correspond to  $\pm 3\sigma_{SN}$ .

22 An optimal agreement is evident in the figure.

23 In order to highlight the small differences between the measured data and the obtained  $FIT$ , we calculated, point-

<sup>3</sup> <http://code.google.com/p/astrolibpy/source/browse/trunk>.

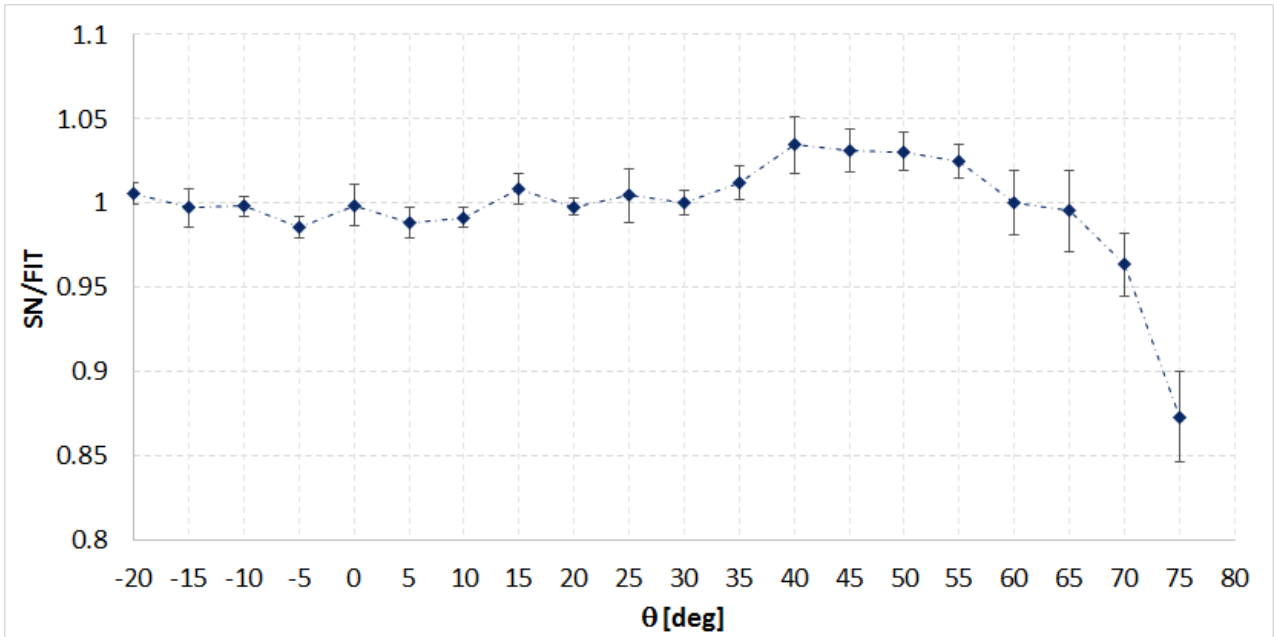
1 by-point, the ratio of the net signal over the fit values by the formula:

$$2 \quad R_i = \frac{SN_i}{FIT_i} \quad (4)$$

3 and we also evaluated the error on each value of  $R$  as:

$$4 \quad \sigma_{RS} = \frac{\sigma_{SN}}{FIT_i} \quad (5)$$

5 The  $R$  values are plotted in Figure 13, where the error bars are  $\pm 3\sigma$ .



6  
7 Figure 13. Plot of the ratio  $SN/FIT$ .

8 As shown in the plot, once the cosine dependency has been accounted for, the detector response remains constant  
9 (within few percent variation) up to 35 degrees, slightly increases in the 35–60 degree range and drops down to 85%  
10 of the initial value at 75 degrees.

11 Surprisingly, while a decrease of  $R$  for high angles may be foreseen, given the low efficiency of the anti-reflection  
12 (AR) feature of the silicone resin coating for such angles, an increase (even if always limited in a 3% range) can be  
13 noted for angles between 35 and 55 degrees. This trend has been confirmed in several measurements and, in our opin-  
14 ion, can be attributed both to the presence of spurious reflections from parts of the enclosure or from the CAEN box  
15 and to mechanical effects (e.g. misalignment of the rotation axis with respect to detector plane, non linearity of stage  
16 motion, etc.). It should be noted that the application of black screens and foils has not reduced this effect. A possible  
17 different reason can be the variation of the AR coating efficacy with the angle of incidence. All these effects will be  
18 investigated more carefully in future works.

## 19 5. Conclusions and Outlook

20 In this paper, measurement results of a newly available large-area MPPC detector (S13360-6075CS) are reported  
21 and discussed. Compared to previous LCT MPPC series, the new LCT device achieves a significant cross-talk reduc-  
22 tion due to optical trench improvements, and higher photon detection efficiency, due to geometrical fill-factor en-  
23 hancement. In addition, it offers improved photon detection capabilities in the NUV spectral region, contributing to  
24 make this new MPPC particularly suitable for new and challenging applications like CTA. Measurement results show

1 that, even for large area devices, promising performance is achieved as well as for the  $3\times 3\text{-mm}^2$  MPPCs. Finally,  
2 measurements of the MPPC photon response versus the angle of incidence are also reported.

### 3 Acknowledgements

4 This work was supported in part by the ASTRI Flagship Project, financed by the Italian Ministry of Education,  
5 University, and Research (MIUR) and led by the Italian National Institute for Astrophysics (INAF). We gratefully  
6 acknowledge support from the agencies and organizations listed in <http://www.cta-observatory.org/?q=node/22>.

### 7 References

- 8 [1] D. Marano, *et al.*, “Electro-Optical Characterization of MPPC Detectors for the ASTRI Cherenkov Telescope Camera”, *Nuclear*  
9 *Instruments and Methods in Physics Research A*, vol. 768, pp. 32-42, 2014.
- 10 [2] G. Pareschi, *et al.*, “The Dual-Mirror Small Size Telescope for the Cherenkov Telescope Array”, *Proceedings ICRC ‘13*, Rio De Janeiro,  
11 Brazil, 2013.
- 12 [3] O. Catalano, *et al.*, “The Camera of the ASTRI SST-2M Prototype for the Cherenkov Telescope Array”, *Proc. SPIE ‘14, Ground-based*  
13 *and Airborne Instrumentation for Astronomy V*, vol. 91470D, Montreal, Canada, 2014.
- 14 [4] S. Vercellone, *et al.*, “The ASTRI Miny-Array Science Case”, *Proceedings ICRC 2013*, Rio De Janeiro, Brazil, July 2013.
- 15 [5] O. Catalano, *et al.*, “The ASTRI SST-2M Prototype: Camera and Electronics”, *Proc. ICRC ‘13*, Rio de Janeiro, 2013.
- 16 [6] B.S. Acharya, *et al.*, “Introducing the CTA Concept”, *Astroparticle Physics*, vol. 43, pp. 3-18, 2013.
- 17 [7] A. Bouvier, *et al.*, “Photosensor Characterization for the Cherenkov Telescope Array: Silicon Photomultiplier versus Multi-Anode  
18 Photomultiplier Tube”, *Proc. SPIE, Hard X-Ray, Gamma-Ray, and Neutron Detector Physics XV*, vol. 8852, San Diego, USA, 2013.
- 19 [8] H. Anderhub *et al.*, “A novel camera type for very high energy gamma-ray astronomy based on Geiger-mode avalanche photodiodes”,  
20 *Journal of Instrumentation*, vol. 4, P10010, 2009.
- 21 [9] H. Anderhub *et al.*, “Design and operation of FACT - the first G-APD Cherenkov telescope”, *Journal of Instrumentation*, vol. 8, P06008,  
22 2013.
- 23 [10] A. Biland, *et al.*, “Calibration and performance of the photon sensor response of FACT - the first G-APD Cherenkov telescope”, *Journal*  
24 *of Instrumentation*, vol. 9, P10012, 2014.
- 25 [11] D. Mazin, *et al.*, “Towards SiPM camera for current and future generations of Cherenkov telescopes”, *Proceedings ICRC ‘13*, Rio De  
26 Janeiro, Brazil, 2013.
- 27 [12] A. Biland, *et al.*, “First detection of air shower Cherenkov light by Geigermode-Avalanche Photodiodes”, *Nuclear Instruments and*  
28 *Methods in Physics Research A*, vol. 595, no. 1, pp. 165-168, 2008.
- 29 [13] N. Otte, *et al.*, “The Potential of SiPM as Photon Detector in Astroparticle Physics Experiments like MAGIC and EUSO”, *Nuclear*  
30 *Physics B – Proceedings Supplements*, vol. 150, pp. 144-149, 2006.
- 31 [14] G. Sottile, *et al.*, “UVSiPM: A Light Detector Instrument Based on a SiPM Sensor Working in Single Photon Counting”, *Nuclear*  
32 *Physics B – Proceedings Supplements*, vol. 239, pp. 258-261, July 2013.
- 33 [15] P. Buzhan, *et al.*, “Silicon Photomultiplier and its Possible Applications”, *Nuclear Instruments and Methods in Physics Research A*, vol.  
34 504, pp. 48-52, 2003.
- 35 [16] S. Siefert, *et al.*, “Ultra Precise Timing with SiPM-Based TOF PET Scintillation Detectors”, *Proc. IEEE Nuclear Science Symposium*  
36 *Conference Records*, pp. 2329-2333, 2009.
- 37 [17] N. Otte, *et al.*, “The SiPM – A new Photon Detector for PET”, *Nuclear Physics B – Proceedings Supplements*, vol. 150, pp. 417-420,  
38 2006.
- 39 [18] P. La Rocca, *et al.*, “Fabrication, Characterization and Testing of Silicon Photomultipliers for the Muon Portal Project”, *Nuclear*  
40 *Instruments and Methods in Physics Research A*, vol. 787, pp. 236-239, 2015.
- 41 [19] F. Riggi, “An Extensive Air Shower Trigger Station for the Muon Portal Detector”, *Nuclear Instruments and Methods in Physics*  
42 *Research A*, vol. 764, pp. 142-149, 2014.
- 43 [20] O. Catalano, *et al.*, “Volcanoes Muon Imaging Using Cherenkov Telescopes”, *Nuclear Instruments and Methods in Physics Research A*,  
44 vol. 807, pp. 5-12, January 2016.
- 45 [21] C. Piemonte, *et al.*, “Characterization of the First Prototypes of Silicon Photomultiplier Fabricated at ITC-irst”, *IEEE Transactions on*  
46 *Nuclear Science*, vol. 54, no. 1, pp. 236-244, 2007.
- 47 [22] K. O’Neill, *et al.*, “SensL B-Series and C-Series silicon photomultipliers for time-of-flight positron emission tomography”, *Nuclear*  
48 *Instruments and Methods in Physics Research A*, vol. 787, no. 1, pp. 169-172, 2015.
- 49 [23] B. Dolgoshein, *et al.*, “Large area UV SiPMs with Extremely Low Cross-Talk”, *Nuclear Instruments and Methods in Physics Research*  
50 *A*, vol. 695, pp. 40-43, 2012.
- 51 [24] C. Jendrysik, *et al.*, “Characterization of the First Prototypes of Silicon Photomultipliers with Bulk-Integrated Quench Resistor  
52 Fabricated at MPI”, *Nuclear Instruments and Methods in Physics Research A*, vol. 718, pp. 262-265, 2013.
- 53 [25] V. Boccone, *et al.*, “Characterization of New Hexagonal Large-Area Geiger Avalanche Photodiodes”, in *Proc. IEEE ANIMMA*, pp. 1-6,  
54 2013.
- 55 [26] G. Bonanno, *et al.*, “Advances in Multi-Pixel Photon Counter Technology: First Characterization Results”, *Nuclear Instruments and*

- 1 *Methods in Physics Research A*, vol. 806, pp. 383-394, January 2016.
- 2 [27] G. Bonanno, *et al.*, "Characterization Measurements Methodology and Instrumental Set-up Optimization for New SiPM Detectors - Part
- 3 II: Optical Tests", *IEEE Sensors Journal*, vol. 14, no. 10, pp. 3567-3578, 2014.
- 4 [28] G. Bonanno, *et al.*, "Characterization Measurements Methodology and Instrumental Set-up Optimization for New SiPM Detectors - Part
- 5 I: Electrical Tests", *IEEE Sensors Journal*, vol. 14, no. 10, pp. 3557-3566, 2014.
- 6 [29] P. Eckert, *et al.*, "Characterisation Studies of Silicon Photomultipliers", *Nuclear Instruments and Methods in Physics Research A*, vol.
- 7 620, no. 1, pp. 217-226, 2010.
- 8 [30] G. Bonanno, *et al.*, "Precision Measurements of Photon Detection Efficiency for SiPM Detectors", *Nuclear Instruments and Methods in*
- 9 *Physics Research A*, vol. 610, pp. 93-97, 2009.
- 10 [31] S. K. Yang, *et al.*, "Precision Measurements of the Photon Detection Efficiency of Silicon Photomultipliers Using Two Integrated
- 11 Spheres", *Optics Express*, vol. 22, no. 1, pp. 716-726, 2014.
- 12 [32] O. Soto, *et al.*, "Characterization of Novel Hamamatsu Multi Pixel Photon Counter (MPPC) Arrays for the GlueX Experiment", *Nuclear*
- 13 *Instruments and Methods in Physics Research A*, vol. 732, pp. 431-436, 2013.
- 14 [33] K. Doroud, *et al.*, "Systematic Study of New Types of Hamamatsu MPPCs Read Out with the NINO ASIC", *Nuclear Instruments and*
- 15 *Methods in Physics Research A*, vol. 753, pp. 149-153, 2014.
- 16 [34] A. Vacherec, *et al.*, "Characterization and Simulation of the Response of Multi-Pixel Photon Counters to Low Light Levels", *Nuclear*
- 17 *Instruments and Methods in Physics Research A*, vol. 656, no. 1, pp. 69-83, 2011.
- 18 [35] P. Buzhan, *et al.*, "The Cross-Talk Problem in SiPMs and Their Use as Light Sensors for Imaging", *Nuclear Instruments and Methods in*
- 19 *Physics Research A*, vol. 610, pp. 131-134, 2009.
- 20 [36] G. Bonanno, *et al.*, "Geiger Avalanche Photodiodes (G-APDs) and Their Characterization, Photodiodes", ISBN: 978-953-307-530-3,
- 21 *InTech*, World Activities in 2011.
- 22 [37] D. Impiombato, *et al.*, "Evaluation of the Optical Cross-Talk Level in the SiPMs Adopted in ASTRI-SST-2M Cherenkov Camera Using
- 23 EASIROC Front-End Electronics", *Journal of Instrumentation*, vol. 9, C02015, 2014.
- 24 [38] D. Marano, *et al.*, "New Improved Model and Accurate Analytical Response of SiPMs Coupled to Read-Out Electronics", *IEEE Sensors*
- 25 *Journal*, vol. 16, no.1, pp. 17-21, 2016.
- 26 [39] F. Villa, *et al.*, "SPICE Electrical Models and Simulations of Silicon Photomultipliers", *IEEE Transactions on Nuclear Science*, vol. 62,
- 27 no. 5, pp. 1950-1960, 2015.
- 28 [40] D. Marano, *et al.*, "Accurate Analytical Single-Photoelectron Response of Silicon Photomultipliers", *IEEE Sensors Journal*, vol. 14, no.
- 29 8, pp. 2749-2754, 2014.
- 30 [41] D. Marano, *et al.*, "Silicon Photomultipliers Electrical Model Extensive Analytical Analysis", *IEEE Transactions on Nuclear Science*,
- 31 vol. 61, no. 1, pp. 23-34, 2014.
- 32 [42] D. Marano, *et al.*, "Improved SPICE Electrical Model of Silicon Photomultipliers", *Nuclear Instruments and Methods in Physics*
- 33 *Research A*, vol. 726, pp. 1-7, 2013.
- 34 [43] S. Vinogradov, *et al.*, "SiPM Response to Long and Intense Pulses", *Nuclear Instruments and Methods in Physics Research A*, vol. 787,
- 35 pp. 148-152, 2015.
- 36 [44] I. Rech, *et al.*, "Optical Crosstalk in Single Photon Avalanche Diode Arrays: A New Complete Model", *Optics Express*, vol. 16, no. 12,
- 37 pp. 8381-8394, 2008.
- 38 [45] J. Fleury, *et al.*, "Petiroc and Citiroc: front-end ASICs for SiPM read-out and ToF applications", *Journal of Instrumentation*, vol. 9, no.
- 39 1, 2014.
- 40 [46] D. Marano, *et al.*, "CITIROC High-Level Analog Front-End Model Implementation and Simulations", *International Journal of Circuits,*
- 41 *Systems and Signal Processing*, vol. 8, pp. 274-285, 2014.
- 42 [47] D. Impiombato, *et al.*, "Characterization and Performance of the ASIC (CITIROC) Front-End of the ASTRI Camera", *Nuclear*
- 43 *Instruments and Methods in Physics Research A*, vol. 794, pp. 185-192, 2015.
- 44 [48] S. Callier, *et al.*, "EASIROC, An Easy & Versatile Readout Device for SiPM", in *Proc. TIPP*, 2001.
- 45 [49] D. Marano, *et al.*, "PSPICE High-Level Model and Simulations of the EASIROC Analog Front-End", *International Journal of*
- 46 *Modelling and Simulations*, vol. 34, no. 4, 2015.
- 47 [50] D. Impiombato, *et al.*, "Characterization of EASIROC as Front-End for the Read-out of the SiPM at the Focal Plane of the Cherenkov
- 48 Telescope ASTRI", *Nuclear Instruments and Methods in Physics Research A*, vol. 729, pp. 484-490, 2013.
- 49 [51] D. Impiombato, *et al.*, "Characterization of the Front-End EASIROC for Read-Out of SiPM in the ASTRI Camera", *Nuclear Physics B -*
- 50 *Proceedings Supplements*, vol. 239, pp. 254-257, 2013.